

Article

Rational Design of Cyclodextrin Glycosyltransferase with Improved Hesperidin Glycosylation Activity

Hanchi Chen ^{1,2}, Jiajun Wang ^{1,2}, Yi Liu ^{1,2}, Yongfan Chen ^{1,2}, Chunfeng Wang ^{1,2}, Linjiang Zhu ^{1,2}, Yuele Lu ^{1,2} and Xiaolong Chen ^{1,2,*} 

¹ College of Biotechnology and Bioengineering, Zhejiang University of Technology, Huzhou 313200, China; hchen23@zjut.edu.cn (H.C.); zhulinjiang@zjut.edu.cn (L.Z.); luyuele@zjut.edu.cn (Y.L.)

² Institute of Fermentation Technology, Zhejiang University of Technology, Huzhou 313200, China

* Correspondence: richard_chen@zjut.edu.cn

Abstract: Cyclodextrin glycosyltransferase (CGTase) can catalyze the glycosylation of hesperidin, resulting in α -glycosyl hesperidin with significantly improved water solubility. In this study, a rational design of CGTase to improve its hesperidin glycosylation activity was investigated. The strategy we employed involved docking hesperidin in its near-attack conformation and virtually mutating the surrounding residues, followed by calculating the changes in binding energy using Rosetta flex-ddG. The mutations with a stabilization effect were then subjected to an activity assay. Starting from CGTase-Y217F, we obtained three double-point mutants, Y217F/M351F, Y217F/M351L, and Y217F/D393H, with improved hesperidin glycosylation activities after screening twenty variants. The best variant, Y217F/D393H, exhibited a catalytic activity of 1305 U/g, and its k_{cat}/K_M is 2.36 times higher compared to CGTase-Y217F and 15.14 times higher compared to the wild-type CGTase. Molecular dynamic simulations indicated that hesperidin was repulsed by CGTase-Y217F when bound in a near-attack conformation. However, by introducing a second-point mutation with a stabilization effect, the repulsion effect is weakened, resulting in a reduction in the distances between the bond-forming atoms and, thus, favoring the reaction.

Keywords: cyclodextrin glycosyltransferase; rational design; flex-ddG; hesperidin; glycosylation



Citation: Chen, H.; Wang, J.; Liu, Y.; Chen, Y.; Wang, C.; Zhu, L.; Lu, Y.; Chen, X. Rational Design of Cyclodextrin Glycosyltransferase with Improved Hesperidin Glycosylation Activity. *Catalysts* **2023**, *13*, 885. <https://doi.org/10.3390/catal13050885>

Academic Editors: Kaili Nie, Yu Ji and Chun Shen

Received: 17 April 2023

Revised: 9 May 2023

Accepted: 10 May 2023

Published: 14 May 2023



Copyright: © 2023 by the authors. Licensee MDPI, Basel, Switzerland. This article is an open access article distributed under the terms and conditions of the Creative Commons Attribution (CC BY) license (<https://creativecommons.org/licenses/by/4.0/>).

1. Introduction

Hesperidin is a natural bioflavonoid enriched in citrus peel. As a member of the vitamin P family, hesperidin is functional in regulating the permeability of capillaries [1]. Other activities, such as anti-oxidation [2], anti-inflammation [3], anticancer [4], and regulating blood sugar and cholesterol levels, have also been reported [5,6]. Typical applications of hesperidin include being used as a pharmaceutical to treat hemorrhoids, varicose veins, and lymphedema, as well as in daily products such as cosmetics and functional foods [7–10]. Hesperidin is more bioavailable in its non-glycosylation state, hesperitin, which is formed after oral intake and hydrolysis by gut microbiota [11]. Unfortunately, gut microbiota can hardly process hesperidin as it is nearly insoluble in water [12]. Poor water solubility also causes problems when trying to apply hesperidin in water-based formulations.

Glycosylation has a profound impact on the water solubility of hesperidin, with the water solubility of monoglucosyl hesperidin reaching as high as 1970 g/L. The study of hesperidin glycosylation was first reported by Kometani et al., who applied cyclodextrin glycosyltransferase (CGTase) originated from an alkalophilic *Bacillus* sp. to catalyze the transglycosylation from starch to hesperidin [13]. The final product involves a series of hesperidin glycosides, including its monoglucosyl and oligoglucosyl forms. Following studies have reported the use of a commercial glucoamylase that hydrolyzes hesperidin oligoglucosides selectively to α -monoglucosyl hesperidin [14]. Currently, α -monoglucosyl hesperidin has been applied in skincare products to protect tissues from cold shock and promote skin rejuvenation [15,16].

As an enzyme capable of catalyzing hesperidin glycosylation, CGTase belongs to the glycoside hydrolase 13 (GH13) family, which is a group of carbohydrate-active enzymes that act on hydrolyzing and transferring α -glucoside linkages through a retaining mechanism [17]. The GH13 family is the largest glycoside hydrolase family, with over 150,000 identified enzymes [18]. It is noteworthy that, in addition to hesperidin, enzymes in the GH13 family have been extensively used to glycosylate a variety of aglycons, including glycerol [19], L-ascorbic acid [20], hydroquinone [21], resveratrol [22], ginsenoside [23], etc., and are deemed industrially important enzymes to synthesize valuable glycosides.

On the other hand, hesperidin glycosylation catalyzed by wild-type CGTase has poor efficiency, with a $k_{\text{cat}}/K_{\text{m}}$ value of 0.07 g/L·min, as investigated in our previous study [24]. To improve the synthetic rate, we applied a size/polarity-guided triple-code strategy to engineer the +1 and +2 subsites, as such areas closely interact with aglycon during transglycosylation. Three residues, F205, Y217, and G283, were identified to significantly impact the catalytic rate, and the change in binding energy of hesperidin in its near-attack conformation in the catalytic pocket appears to be the key reason [24].

Binding energy refers to the energy required to bring and stabilize a ligand molecule into an active site. Ignoring inactive binding states, the energy required for a ligand to bind in its near-attack conformation contributes significantly to the overall energy barrier and can, therefore, serve as a valuable reference during enzyme design [25]. In this work, we started with our previous mutant CGTase-Y217F and attempted to identify more key residues rationally by calculating the change in binding energy after virtual mutations using flex-ddG, a Rosetta-based modeling suit [26]. After screening 20 mutants, 3 positive mutants were obtained, and M351 and D393 were identified as two new key residues.

2. Results

2.1. Selection of Mutagenesis Sites and Rational Design

The crystal structure of CGTase studied in this research (NCBI accession number: BAA31539.1) has not yet been resolved. However, the crystal structure of CGTase from *Bacillus circulans* strain 251, which shares 73.6% sequence similarity, is available (PDB: 1CXL) in a covalent complex with a glycosyl donor [27]. Using this as a reference, a theoretical model of CGTase was constructed, and molecular docking was performed to obtain the structure model of CGTase-Y217F in a complex with hesperidin, as shown in Figure 1a.

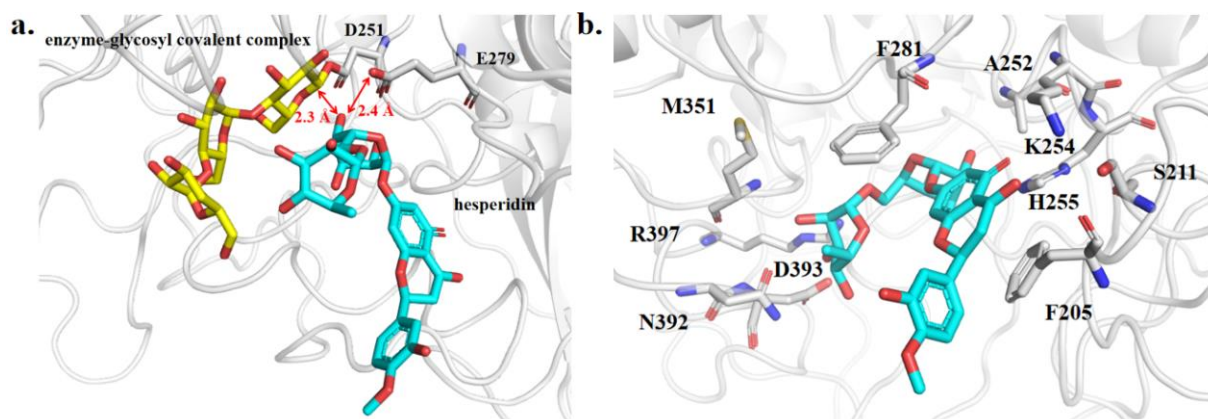


Figure 1. (a) Hesperidin docked with the enzyme–glycosyl covalent complex. The structure model of CGTase-Y217F was constructed by SWISS-MODEL using a crystal structure (PDB: 1CXL) as a template. (b) 10 residues within a 4 Å radius of hesperidin were selected for rational design.

The catalytic process is driven by a double-displacement mechanism that is catalyzed by a catalytic triad consisting of D251, E279, and D350. In this process, D251 and E279 play the roles of electron donors and acceptors, respectively. D350, on the other hand, does not participate in the reaction but instead serves to accurately position the glucose unit at the -1 position [27]. In this case, in addition to the catalytic triad and the first-generation

mutagenesis (Y217F), ten residues within a 4 Å radius of the docked hesperidin were selected for rational design, which include F205, S211, A252, K254, H255, F281, M351, N392, D393, and R397 (Figure 1b). A saturated virtual mutation was applied to these selected residues, and the change in binding energies before and after the mutation was calculated using Rosetta flex-ddG. Figure 2 shows the results that are considered to stabilize hesperidin in its near-attack binding conformation ($\Delta\Delta G \leq -1.0$ kcal/mol), which are subjected to mutagenesis and an assay. The entire calculation results are given in the Supplementary Materials Section (Figure S1).

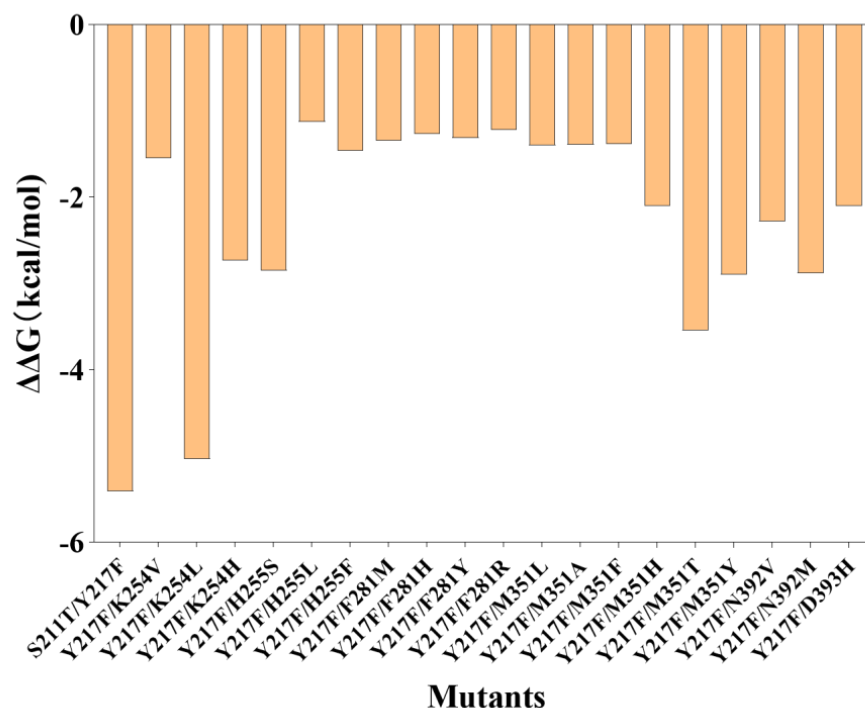


Figure 2. Mutations with stabilization effect calculated by Rosetta flex-ddG.

2.2. Library Construction and Screening

A mutagenesis library was constructed using pET-22b(+)/CGTase-Y217F-6×His as the template and corresponding primers for each of the 20 designed mutants. The resulting plasmids were confirmed to carry the CGTase-expressing gene through gel electrophoresis (Figure S2), and the target mutations were confirmed by DNA sequencing.

The activities of heterogeneously expressed CGTases were assayed through two consecutive rounds of screening, either using whole cells or purified enzymes. SDS-PAGE was applied to characterize the purified enzymes (Figure S3). The screening results are shown in Table 1. The mutations at M351 and D393 were found to favor the target reaction. The specific transglycosylation activities of the positive mutants Y217F/M351F, Y217F/M351L, and Y217F/D393H were assayed to be 1171 U/g, 1126 U/g, and 1305 U/g, which are 1.25, 1.20, and 1.39 times higher compared to the first-generation mutant Y217F and significantly superior than the wild-type CGTase (134 U/g). The disproportion kinetics of the three positive variants were analyzed, as shown in Table 2, based on a ping-pong mechanism. In the case of k_{cat}/K_{mA} , representing the enzymes' hesperidin glycosylation ability in abundance of maltodextrin, the best variant Y217F/D393H is 2.36 times higher than Y217F and 15.14 times higher compared to the wild type. The original kinetic data are displayed in Figure S4.

Table 1. Activities of CGTase variants assayed with whole cells (relative activity) and purified enzymes (specific activity).

Enzyme	Relative Activity (%)	Specific Transglycosylation Activity (U/g)
WT	100	134.4 ± 7.0
Y217F	671.6	916.6 ± 22.2
S211T/Y217F	574.2	-
Y217F/K254V	458.1	-
Y217F/K254L	684.1	478.3 ± 20.7
Y217F/K254H	575.6	-
Y217F/H255S	16.3	-
Y217F/H255L	89.4	-
Y217F/H255F	41.4	-
Y217F/F281M	333.1	-
Y217F/F281Y	743.3	805.6 ± 6.3
Y217F/F281R	68.2	-
Y217F/F281H	157.9	-
Y217F/M351T	402.5	-
Y217F/M351F	774.5	1194.7 ± 12.5
Y217F/M351L	791.8	1126.1 ± 6.4
Y217F/M351A	287.5	-
Y217F/M351Y	547.0	-
Y217F/M351H	238.0	-
Y217F/N392V	533.8	-
Y217F/N392M	474.4	-
Y217F/D393H	716.4	1306.4 ± 21.6

Table 2. Disproportion kinetics of the wild-type CGTase and its variants.

Enzyme	k_{cat} (min^{-1})	K_{mA} (Hesperidin) (g/L)	K_{mB} (Maltodextrin) (g/L)	k_{cat}/K_{mA} (L/g·min)
WT	0.47	6.52	0.92	0.07
Y217F	4.85	10.86	2.11	0.45
Y217F/M351F	11.58	16.43	6.48	0.71
Y217F/M351L	16.31	26.42	4.87	0.62
Y217F/D393H	14.74	13.87	2.84	1.06

3. Discussions

The primary application of CGTases is to produce cyclodextrins, which are macrocyclic molecules used to encapsulate other molecules, resulting in the formation of inclusion complexes with improved water solubility and stability [28]. Recently, the use of CGTase to catalyze intermolecular transglycosylation has attracted wide attention as the reaction uses cheap glycosyl donors, such as starch and maltodextrin, to produce valuable glycosides. Besides hesperidin, the glycosylation of its aglycon, hesperitin, using CGTase has also been reported [29]. Several studies have reported the engineering of CGTase to improve its ability to catalyze intermolecular glycosylation reactions. For example, Han et al. applied site-saturation mutagenesis to K47 of CGTase from *Paenibacillus macerans* and improved the yield of AA-2G, a glycosylation product of L-ascorbic acid, by 64.2% [30]. Tao et al. engineered the residues near the catalytic site, and the enzyme's k_{cat}/K_m in synthesizing AA-2G was increased by 2.69-fold [31]. Han et al. engineered the nonconservative site of CGTase and improved its selectivity for synthesizing long-chain glycosylated sophoricosides [32]. Ara et al. engineered three residues near the acceptor subsites and obtained variants with improved coupling activities for synthesizing alkyl glycosides with elongated carbohydrate chains [33].

Although previous studies have been successful in regulating intermolecular glycosylation abilities, rational engineering of a CGTase based on a target transglycosylation reaction has not yet been achieved. It is worth noting that several methods have been proposed to rationally design an enzyme, which are based on the principle of reducing activation energy by minimizing the energy of the enzyme–ligand complex along the

reaction pathway but with different algorithms. For instance, a fixed-backbone design only permits side-chain rotamers to be varied during enzyme design while keeping the backbone conformation fixed [34]. In contrast, a backrub design allows for backbone conformational variations before designing for each member of the ensemble [35]. Although fixed-backbone design is computationally efficient, backrub design samples the flexibility in enzyme structure that is closer to the real case of enzymatic catalysis and theoretically provides more accurate results.

In a previous study, we engineered the aglycon-attacking site of CGTase from the alkalophilic *Bacillus* sp. A2-5a and obtained eight positive mutants at three sites [24]. Upon characterizing the positive effects, it became apparent that the stabilization of hesperidin in its near-attack conformation was the major contributing factor. In this case, we started with the best first-generation mutant Y217F and further applied a flex-ddG design inoculated with the backrub algorithm in this study, aiming to identify additional residues whose mutations could potentially contribute to the energy profile along the glycosylation pathway.

The CGTase-catalyzed glycosylation of hesperidin proceeds through a double-displacement mechanism, where hesperidin attacks the enzyme–glycosyl intermediate from the reducing end in the second displacement step, ultimately leading to the formation of an α -1,4-glucosidic bond (Figure 3) [27]. In the docked structure shown in Figure 1a, the glucose unit of hesperidin is positioned beneath the glycosyl intermediate chain, with the nucleophile O_4 2.3 Å away from C_α , and the distance between the electron donor, OE2 in E279, and H4 in hesperidin is 2.4 Å. These distances fall within the average van der Waals distance between carbon and oxygen (3.35 Å) and oxygen and hydrogen (2.6 Å), indicating that the bond-forming atoms are within near-attack distance to form an α -1,4-glucosidic bond. Based on this observation, the selected docked structure has the potential to be developed for the target reaction, and a rational design aimed at promoting the formation of this structure could potentially benefit the reaction.

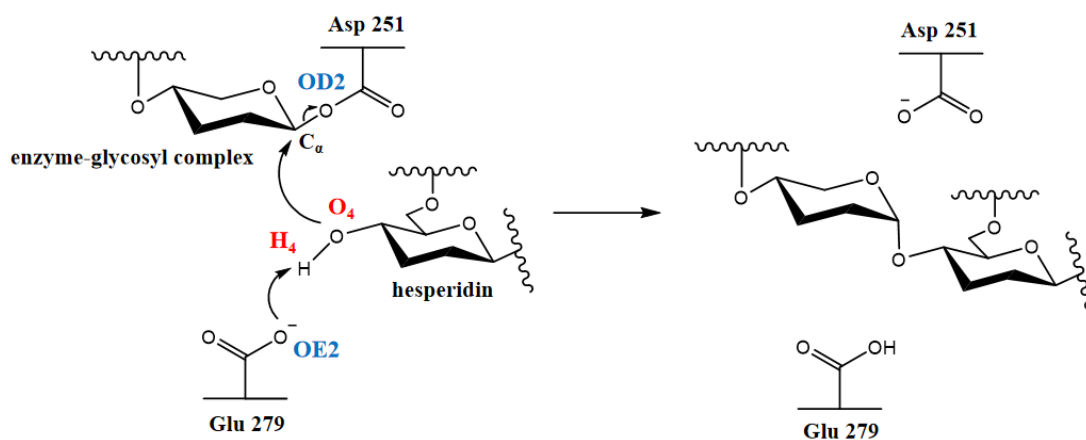


Figure 3. The mechanism of hesperidin glycosylation catalyzed by CGTase.

Based on the design and screening results, when using the near-attack conformation as the starting structure, a total of twenty designs demonstrated stabilization effects, and three were screened to be positive. It is important to note that rational design at the current stage may not achieve 100% accuracy due to several reasons. For instance, Lodola et al. demonstrated that amide hydrolysis by an amide hydrolase occurs more readily in a high-energy conformation than in the ground state [36]. Additionally, Romero-Télez et al. suggested that, due to the flexibility of the enzyme–ligand complex, the energy barrier of an enzyme-catalyzed reaction is not determined by a single reaction pathway [37]. The different precatalytic structures may result in a dispersion of energy barriers that combine statistically to determine the reaction kinetics. Thus, due to the conformational effect, rational design from a static Michaelis complex structure, which is usually used as the starting point for rational design, may not capture the full picture of the catalytic mechanism. Wijma et al. investigated the rational design of the enantioselectivity of an epoxide hydrolase [38]. They propose to further evaluate the designed mutant by high-

throughput molecular dynamic simulation to further confirm the frequency of forming near-attack conformations.

To gain a deeper understanding of the positive effect, we conducted molecular dynamic simulations on CGTase-Y217F and the three identified positive mutants. The relative positions of the atoms involved in bond formation play a crucial role in determining the likelihood of their effective collision, which is critical for the success of the reaction. By fixing the relative positions of C_{α} and OD2 in Asp251, we determined the distances between the bond-forming atoms, as shown in Figure 4. During the 10 ns simulation, the distances between the bond-forming atoms increased, suggesting repulsion between the two molecules. Our previous study showed that although the Y217F point mutation removes the bump at the pocket entrance and facilitates hesperidin transportation, it has a destabilizing effect on hesperidin binding. In this case, introducing mutations with stabilization effects, as performed in this study, can potentially overcome the Y217F mutation's defect and further improve the enzyme's catalytic performance. By introducing mutations at M351 and D393, the repulsion effect is weakened and the average distances between the bond-forming atoms are reduced, as shown in Table 3, which explains the positive effect observed.

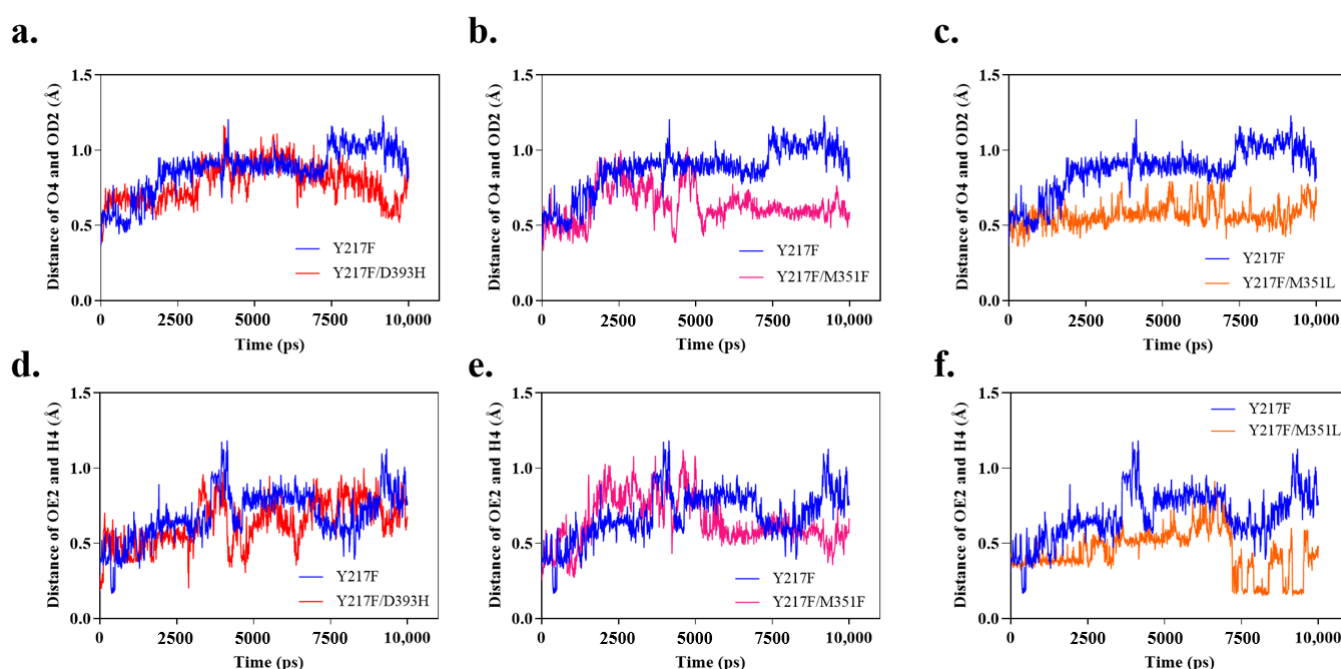


Figure 4. (a–f) The distances of bond-forming atoms during molecular dynamic simulation.

Table 3. Average distances between bond-forming atoms during 10 ns simulation.

Mutants	Average Distances during 10 ns Simulation (Å)	
	O ₄ and C _α	H ₄ and OE2 in E279
Y217F	0.832	0.686
Y217F/M351F	0.540	0.645
Y217F/M351L	0.531	0.444
Y217F/D393H	0.729	0.634

4. Materials and Methods

4.1. Materials, Plasmids, and Strains

The nucleotide sequence encoding CGTase (NCBI accession number: BAA31539.1) was synthesized with a polyhistidine tag attached on the C-terminus [39]. Recombinant vectors and strains were obtained following previously reported protocols [24]. Hesperidin, dextrin, and other chemicals were purchased from Sinopharm Chemical Reagent Co., Ltd. (Shanghai, China). His60 Ni Superflow resin and gravity columns were purchased from

SunResin Co. (Xi'an, China). Genetic engineering reagents, including a Super-Fidelity DNA Polymerase Kit, *Dpn* I digesting enzyme, and a One Step Cloning Kit, were purchased from Vazyme Biotech (Nanjing, China).

4.2. Structure Modeling and Rational Design

The theoretical structure of CGTase-Y217F in a complex with hesperidin was obtained in our previous study [24]. Residues within the 4 Å radius of the docked ligand were virtually mutated to the other 19 common amino acids, and changes in the ligand binding energy after mutation were calculated using Rosetta flex-ddG. Results with $\Delta\Delta G \leq -1.0$ kcal/mol were employed for mutagenesis and an activity assay. The user-defined options in Rosetta flex-ddG include the following: repetitive computation: “nstruct = 15”; max minimization gradient descent steps: “max_minimization_iter” = 5000; maximum allowed score change threshold of minimization: “abs_score_convergence_thresh” = 1.0; number of backrub sampling steps: “number_backrub_trials” = 35000; steps of ddG calculation during backrub: “backrub_trajectory_stride” = 35000; residue to mutate: “residue_to_mutate = (‘protein chain name’, ‘residue number’)”; target mutation: “mut_aa in ‘ACDEFGHIKLMNPQRSTVWY’”. A “chain_to_move.txt” file was written to define the ligand molecule.

4.3. Preparation of Mutant Libraries

Primers were synthesized as listed in Table 4. The target mutation was constructed by amplifying the entire plasmid pET-22b(+)/CGTase-6×His using the corresponding primers. The PCR conditions were followed according to the instructions of the Phanta[®] Max Super-Fidelity DNA Polymerase Kit (Vazyme Biotech, Nanjing, China). The PCR product was then digested with *Dpn* I (Vazyme Biotech, Nanjing, China) and circulated with the One Step Cloning Kit (Vazyme Biotech, Nanjing, China), leading to a plasmid with the target mutation. The plasmid was then transformed into competent *E. coli* BL21 (DE3) cells. The above procedures were repeated with different primers to create libraries with CGTase mutants for screening.

Table 4. Primers used for point mutations.

Primers	Sequence (5′–3′ Direction) xxx: Mutation Site	Target Mutation (Codon)					
S211-R	aatctgttgatctggcggattacgatctg	T					
S211-F	cgccagatcaaacagattgcggtaaatxxxatcctcata	ggt					
K254-R	ttgatggcattcgctggatgcggtxxxacatgagcgaag	V	L	H			
K254-F	tccacgcgaatgcatcaatgctttgtcca	gtg	cat	ctg			
H255-R	gaaggctggcagactagcctgatgagcgatatt	S	L	F			
H255-F	gctagtctgccagccttgcctcatxxxtttaac	gct	cag	gaa			
F281-R	agcggcgaagttgatccgagaacatcat	M	Y	R	H		
F281-F	cggatcaactcgcgctgccagxxxccattc	cat	ata	gcg	atg		
M351-R	agcggcgaagttgatccgagaacatcat	T	F	L	A	Y	H
M351-F	gctctgttcaagctaaagcggctxxxgtcatggtt	cgt	gaa	cag	cgc	ata	atg
N392-R	gaaaaccgcaaaccgatgagcgattttgat	V	M				
N392-F	tcatcggtttcggtttccggatcxxxgcccgcctcagat	cac	cat				
D393-R	gaaaaccgcaaaccgatgagcgattttgat	H					
D393-F	atcggtttcggtttccggxxxattgccgccctcagata	atg					

4.4. Screening of Positive Mutants

Two rounds of screening were performed to assay the enzyme activities using whole cells and purified enzymes. In the first round of screening, recombinant *E. coli* BL21 (DE3) cells were inoculated into 50 mL aliquots of LB medium with 10 g/L glycerol and 100 mg/L ampicillin in shake flasks. After culturing at 37 °C for 6 h, 50 µL of IPTG (500 mM)

was supplemented, and the incubation temperature was reduced to 22 °C for enzyme expression. After another 4 h of culturing, the cells were harvested, and the OD₆₀₀ of each culture was determined. Whole-cell catalysis was performed for 60 min with the culture at 40 °C and pH = 10.0, adjusted by 1M NaOH. Dextrin (100 g/L; DE = 13.31, determined by the DNS method) and hesperidin (10 g/L) were supplemented as glycosyl donors and acceptors, respectively. The samples were added to 1M NaOH to quench the reaction. The concentration of hesperidin and its glycosylation products were determined by HPLC with an InertSustain C18 (GL Sciences, Tokyo, Japan) column. One unit of whole-cell transglycosylation activity (WCTA) was defined as 1 μmol of substrate converted per minute by a unit concentration of cells. The mutants with WCTA larger than CGTase-Y217F were subjected to a second round of screening.

In the second round of screening, the purified CGTases were obtained using His60 Ni Superflow resin and gravity columns. The purity of the obtained CGTases was confirmed by SDS-PAGE, and the protein concentrations were determined by the Bradford method. The enzyme activities were assayed by adding 20 μL of enzyme to a 2 mL solution containing dextrin (100 g/L; DE = 13.31) and hesperidin (10 g/L). The reactions were conducted at 40 °C for 15 min at pH = 10.0, adjusted by 1M NaOH. The samples were added to 1 M NaOH to quench the reaction and then analyzed by HPLC. One unit of specific enzyme activity was defined as 1 μmol of substrate converted per minute by a unit concentration of enzyme.

4.5. Kinetic Analysis

The glycosylation kinetics were investigated with the purified CGTases. The reaction was initiated by adding 20 μL of enzyme to a 2 mL solution containing hesperidin and maltodextrin in various concentrations. Catalysis was performed at 40 °C and pH = 10.0 for 15 min to determine the initial rates. The obtained experimental data were fit to Equation (1) on behalf of a ping-pong mechanism, where v (g/L·min) stands for the disproportion rate, E_0 is the enzyme concentration, and $[A]$ and $[B]$ stand for the hesperidin and maltodextrin concentrations (g/L), respectively.

$$v = \frac{k_c E_0 [A][B]}{K_{mB}[A] + K_{mA}[B] + [A][B]} \quad (1)$$

4.6. Molecular Dynamic Analysis

Gromacs was employed for a molecular dynamic analysis. The theoretical structure of CGTase-Y217F with hesperidin docked in its near-attack conformation was used as the starting structure. The theoretical structures of the mutants were generated with FoldX. The starting structure was solvated in a dodecahedron box with a TIP3P water model. Na⁺ and Cl⁻ ions were used for system neutralization. A CHARMM36 forcefield was applied for protein topology generation and ligand parameterization [40]. The starting structure was first minimized with the steepest descent algorithm until a maximum force lower than 10 kJ/mol·nm was reached. The system was then equilibrated in an NVT ensemble at 300 K for 50,000 steps, 2 fs for each step. The non-bonded interactions were cut off at 12 Å and updated every 20 steps. Another equilibration was performed in an NPT ensemble with the same parameters. A dynamic simulation was then conducted for 10 ns, with the coordinates saved every 10 ps.

5. Conclusions

Rational enzyme design typically involves the steps of docking a ligand in its near-attack conformation, selecting surrounding residues, and calculating binding energies after virtual mutations. Although achieving absolute design accuracy is difficult, this protocol usually generates an operable and referable library. In this study, we aimed to further improve the hesperidin glycosylation activity of our previously obtained single-point mutant CGTase-Y217F by rationally designing the enzyme using Rosetta flex-ddG. A library of twenty variants was designed, and three were found to have improved activity.

A molecular dynamic simulation showed that introducing a second-point mutation with a stabilization effect kept the bond-forming atoms closer together and significantly reduced repulsion between the enzyme and hesperidin.

Supplementary Materials: The following supporting information can be downloaded at <https://www.mdpi.com/article/10.3390/catal13050885/s1>, Figure S1: Using CGTase-Y217F as template, change of hesperidin binding energy calculated after saturated virtual mutation of selected residues; Figure S2: Agarose gel electrophoresis of the designed 20 mutants; Figure S3: SDS-PAGE of purified CGTase variants; Figure S4: Linearly regressed Lineweaver-Burk plot based on ping-pong mechanism.

Author Contributions: Conceptualization, H.C., L.Z. and Y.L. (Yuele Lu); methodology, H.C. and Y.L. (Yi Liu); software, H.C.; validation, J.W., Y.L. (Yi Liu), Y.C. and C.W.; formal analysis, H.C.; investigation, H.C.; resources, H.C.; data curation, H.C.; writing—original draft preparation, H.C.; writing—review and editing, H.C.; visualization, H.C.; supervision, X.C.; project administration, H.C. and X.C.; funding acquisition, X.C. All authors have read and agreed to the published version of the manuscript.

Funding: This research was funded by the National Natural Science Foundation of China (21908196) and the National Ten Thousand Talent Program (2017).

Data Availability Statement: Nucleotide and amino acid sequence of the wild-type CGTase are available at NCBI (accession number BAA31539.1). Other data support this study are available from the corresponding author upon reasonable request.

Conflicts of Interest: The authors declare no conflict of interest.

References

1. Garg, A.; Garg, S.; Zaneveld, L.J.D.; Singla, A.K. Chemistry and pharmacology of the citrus bioflavonoid hesperidin. *Phytother. Res.* **2001**, *15*, 655–669. [[CrossRef](#)] [[PubMed](#)]
2. Wilmsen, P.K.; Spada, D.S.; Salvador, M. Antioxidant activity of the flavonoid hesperidin in chemical and biological systems. *J. Agric. Food. Chem.* **2005**, *53*, 4757–4761. [[CrossRef](#)] [[PubMed](#)]
3. Parhiz, H.; Roohbakhsh, A.; Soltani, F.; Rezaee, R.; Iranshahi, M. Antioxidant and anti-inflammatory properties of the citrus flavonoids hesperidin and hesperetin: An updated review of their molecular mechanisms and experimental models. *Phytother. Res.* **2015**, *29*, 323–331. [[CrossRef](#)] [[PubMed](#)]
4. Devi, K.P.; Rajavel, T.; Nabavi, S.F.; Setzer, W.N.; Ahmadi, A.; Mansouri, K.; Nabavi, S.M. Hesperidin: A promising anticancer agent from nature. *Ind. Crops Prod.* **2015**, *76*, 582–589. [[CrossRef](#)]
5. Al-Ishaq, R.K.; Abotaleb, M.; Kubatka, P.; Kajo, K.; Büsselberg, D. Flavonoids and their anti-diabetic effects: Cellular mechanisms and effects to improve blood sugar levels. *Biomolecules* **2019**, *9*, 430. [[CrossRef](#)]
6. Wang, X.; Hasegawa, J.; Kitamura, Y.; Wang, Z.; Matsuda, A.; Shinoda, W.; Miura, N.; Kimura, K. Effects of hesperidin on the progression of hypercholesterolemia and fatty liver induced by high-cholesterol diet in rats. *J. Pharmacol. Sci.* **2011**, *117*, 129–138. [[CrossRef](#)]
7. Li, C.; Schluesener, H. Health-promoting effects of the citrus flavanone hesperidin. *Crit. Rev. Food Sci. Nutr.* **2017**, *57*, 613–631. [[CrossRef](#)]
8. Stanisic, D.; Liu, L.H.; Dos Santos, R.V.; Costa, A.F.; Durán, N.; Tasic, L. New sustainable process for hesperidin isolation and anti-ageing effects of hesperidin nanocrystals. *Molecules* **2020**, *25*, 4534. [[CrossRef](#)]
9. Mayneris-Perxachs, J.; Alcaide-Hidalgo, J.M.; de la Hera, E.; del Bas, J.M.; Arola, L.; Caimari, A. Supplementation with biscuits enriched with hesperidin and naringenin is associated with an improvement of the Metabolic Syndrome induced by a cafeteria diet in rats. *J. Funct. Foods* **2019**, *61*, 103504. [[CrossRef](#)]
10. Valls, R.M.; Pedret, A.; Calderón-Pérez, L.; Llauro, E.; Pla-Pagà, L.; Companys, J.; Moragas, A.; Martín-Luján, F.; Ortega, Y.; Giralt, M.; et al. Hesperidin in orange juice improves human endothelial function in subjects with elevated blood pressure and stage 1 hypertension: A randomized, controlled trial (Citrus study). *J. Funct. Foods* **2021**, *85*, 104646. [[CrossRef](#)]
11. Wdowiak, K.; Walkowiak, J.; Pietrzak, R.; Bazan-Woźniak, A.; Cielecka-Piontek, J. Bioavailability of Hesperidin and Its Aglycone Hesperetin—Compounds Found in Citrus Fruits as a Parameter Conditioning the Pro-Health Potential (Neuroprotective and Antidiabetic Activity)—Mini-Review. *Nutrients* **2022**, *14*, 2647. [[CrossRef](#)] [[PubMed](#)]
12. Anwer, M.K.; Al-Shdefat, R.; Jamil, S.; Alam, P.; Abdel-Kader, M.S.; Shakeel, F. Solubility of bioactive compound hesperidin in six pure solvents at (298.15 to 333.15) K. *J. Chem. Eng. Data* **2014**, *59*, 2065–2069. [[CrossRef](#)]
13. Kometani, T.; Terada, Y.; Nishimura, T.; Takii, H.; Okada, S. Transglycosylation to hesperidin by cyclodextrin glucanotransferase from an alkalophilic *Bacillus* species in alkaline pH and properties of hesperidin glycosides. *Biosci. Biotechnol. Biochem.* **1994**, *58*, 1990–1994. [[CrossRef](#)]
14. Choi, S.S.; Lee, S.H.; Lee, K.A. A comparative study of hesperetin, hesperidin and hesperidin glucoside: Antioxidant, anti-inflammatory, and antibacterial activities in vitro. *Antioxidants* **2022**, *11*, 1618. [[CrossRef](#)] [[PubMed](#)]

15. Lee, Y.S.; Woo, J.B.; Ryu, S.I.; Moon, S.K.; Han, N.S.; Lee, S.B. Glucosylation of flavonol and flavanones by *Bacillus* cyclodextrin glucosyltransferase to enhance their solubility and stability. *Food Chem.* **2017**, *229*, 75–83. [[CrossRef](#)] [[PubMed](#)]
16. Yamada, M.; Tanabe, F.; Arai, N.; Mitsuzumi, H.; Miwa, Y.; Kubota, M.; Chaen, H.; Kibata, M. Bioavailability of glucosyl hesperidin in rats. *Biosci. Biotechnol. Biochem.* **2006**, *70*, 1386–1394. [[CrossRef](#)]
17. Janecek, Š.; Svensson, B.; MacGregor, E. α -Amylase: An enzyme specificity found in various families of glycoside hydrolases. *Cell. Mol. Life Sci.* **2014**, *71*, 1149–1170. [[CrossRef](#)]
18. Lombard, V.; Golaconda Ramulu, H.; Drula, E.; Coutinho, P.M.; Henrissat, B. The carbohydrate-active enzymes database (CAZy) in 2013. *Nucleic Acids Res.* **2014**, *42*, D490–D495. [[CrossRef](#)]
19. Zhou, J.; Jiang, R.; Shi, Y.; Ma, W.; Liu, K.; Lu, Y.; Zhu, L.; Chen, X. Sucrose phosphorylase from *Lactobacillus reuteri*: Characterization and application of enzyme for production of 2-O- α -d-glucopyranosyl glycerol. *Int. J. Biol. Macromol.* **2022**, *209*, 376–384. [[CrossRef](#)]
20. Zhou, Y.; Gan, T.; Jiang, R.; Chen, H.; Ma, Z.; Lu, Y.; Zhu, L.; Chen, X. Whole-cell catalytic synthesis of 2-O- α -glucopyranosyl-L-ascorbic acid by sucrose phosphorylase from *Bifidobacterium breve* via a batch-feeding strategy. *Process Biochem.* **2022**, *112*, 27–34. [[CrossRef](#)]
21. Yu, S.; Wang, Y.; Tian, Y.; Xu, W.; Bai, Y.; Zhang, T.; Mu, W. Highly efficient biosynthesis of α -arbutin from hydroquinone by an amylosucrase from *Cellulomonas carboniz.* *Process Biochem.* **2018**, *68*, 93–99. [[CrossRef](#)]
22. Marié, T.; Willig, G.; Teixeira, A.R.; Gazaneo Barboza, E.; Kotland, A.; Gratia, A.; Courot, E.; Hubert, J.; Renault, J.H.; Allais, F. Enzymatic synthesis of resveratrol α -glycosides from β -cyclodextrin-resveratrol complex in water. *ACS Sustain. Chem. Eng.* **2018**, *6*, 5370–5380. [[CrossRef](#)]
23. Moon, S.S.; Lee, H.J.; Mathiyalagan, R.; Kim, Y.J.; Yang, D.U.; Lee, D.Y.; Min, J.W.; Jimenez, Z.; Yang, D.C. Synthesis of a novel α -glucosyl ginsenoside F1 by cyclodextrin glucanotransferase and its in vitro cosmetic applications. *Biomolecules* **2018**, *8*, 142. [[CrossRef](#)] [[PubMed](#)]
24. Chen, H.; Liu, Y.; Ren, X.; Wang, J.; Zhu, L.; Lu, Y.; Chen, X. Engineering of Cyclodextrin Glycosyltransferase through a Size/Polarity Guided Triple-Code Strategy with Enhanced α -Glycosyl Hesperidin Synthesis Ability. *Appl. Environ. Microbiol.* **2022**, *88*, e01027-22. [[CrossRef](#)] [[PubMed](#)]
25. Hur, S.; Bruice, T.C. The near attack conformation approach to the study of the chorismate to prephenate reaction. *Proc. Natl. Acad. Sci. USA* **2003**, *100*, 12015–12020. [[CrossRef](#)] [[PubMed](#)]
26. Barlow, K.A.; Conchúir, S.Ó.; Thompson, S.; Suresh, P.; Lucas, J.E.; Heinonen, M.; Kortemme, T. Flex ddG: Rosetta ensemble-based estimation of changes in protein–protein binding affinity upon mutation. *J. Phys. Chem. B* **2018**, *122*, 5389–5399. [[CrossRef](#)]
27. Uitdehaag, J.; Mosi, R.; Kalk, K.H.; van der Veen, B.A.; Dijkhuizen, L.; Withers, S.G.; Dijkstra, B.W. X-ray structures along the reaction pathway of cyclodextrin glycosyltransferase elucidate catalysis in the α -amylase family. *Nat. Struct. Biol.* **1999**, *6*, 432–436. [[CrossRef](#)]
28. Szejtli, J. Past, Present and future of cyclodextrin research. *Pure Appl. Chem.* **2004**, *76*, 1825–1845. [[CrossRef](#)]
29. González-Alfonso, J.L.; Míguez, N.; Padilla, J.D.; Leemans, L.; Poveda, A.; Jiménez-Barbero, J.; Ballesteros, A.O.; Sandoval, G.; Plou, F.J. Optimization of regioselective α -glucosylation of hesperetin catalyzed by cyclodextrin glucanotransferase. *Molecules* **2018**, *23*, 2885. [[CrossRef](#)]
30. Han, R.; Liu, L.; Shin, H.D.; Chen, R.R.; Du, G.; Chen, J. Site-saturation engineering of lysine 47 in cyclodextrin glycosyltransferase from *Paenibacillus macerans* to enhance substrate specificity towards maltodextrin for enzymatic synthesis of 2-O-D-glucopyranosyl-L-ascorbic acid (AA-2G). *Appl. Microbiol. Biotechnol.* **2013**, *97*, 5851–5860. [[CrossRef](#)]
31. Tao, X.; Wang, T.; Su, L.; Wu, J. Enhanced 2-O- α -d-glucopyranosyl-L-ascorbic acid synthesis through iterative saturation mutagenesis of acceptor subsite residues in *Bacillus stearothermophilus* NO₂ cyclodextrin glycosyltransferase. *J. Agric. Food. Chem.* **2018**, *66*, 9052–9060. [[CrossRef](#)] [[PubMed](#)]
32. Han, R.; Chai, B.; Jiang, Y.; Ni, J.; Ni, Y. Engineering of cyclodextrin glycosyltransferase from *Paenibacillus macerans* for enhanced product specificity of long-chain glycosylated sophoricosides. *Mol. Catal.* **2022**, *519*, 112147. [[CrossRef](#)]
33. Ara, K.Z.G.; Linares-Pastén, J.A.; Jönsson, J.; Vilorio-Cols, M.; Ulvenlund, S.; Adlercreutz, P.; Karlsson, E.N. Engineering CGTase to improve synthesis of alkyl glycosides. *Glycobiology* **2021**, *31*, 603–612. [[CrossRef](#)] [[PubMed](#)]
34. Pokala, N.; Handel, T.M. Protein design—Where we were, where we are, where we’re going. *J. Struct. Biol.* **2001**, *134*, 269–281. [[CrossRef](#)] [[PubMed](#)]
35. Smith, C.A.; Kortemme, T. Backrub-like backbone simulation recapitulates natural protein conformational variability and improves mutant side-chain prediction. *J. Mol. Biol.* **2008**, *380*, 742–756. [[CrossRef](#)]
36. Lodola, A.; Mor, M.; Zurek, J.; Tarzia, G.; Piomelli, D.; Harvey, J.N.; Mulholland, A.J. Conformational effects in enzyme catalysis: Reaction via a high energy conformation in fatty acid amide hydrolase. *Biophys. J.* **2007**, *92*, L20–L22. [[CrossRef](#)]
37. Romero-Téllez, S.; Cruz, A.; Masgrau, L.; González-Lafont, À.; Lluch, J.M. Accounting for the instantaneous disorder in the enzyme–substrate Michaelis complex to calculate the Gibbs free energy barrier of an enzyme reaction. *Phys. Chem. Chem. Phys.* **2021**, *23*, 13042–13054. [[CrossRef](#)]
38. Wijma, H.J.; Floor, R.J.; Bjelic, S.; Marrink, S.J.; Baker, D.; Janssen, D.B. Enantioselective enzymes by computational design and in silico screening. *Angew. Chem. Int. Ed.* **2015**, *54*, 3726–3730. [[CrossRef](#)]
39. Ohdan, K.; Kuriki, T.; Takata, H.; Okada, S. Cloning of the cyclodextrin glucanotransferase gene from alkalophilic *Bacillus* sp. A2-5a and analysis of the raw starch-binding domain. *Appl. Microbiol. Biotechnol.* **2000**, *53*, 430–434. [[CrossRef](#)]

40. Huang, J.; MacKerell, A.D., Jr. CHARMM36 all-atom additive protein force field: Validation based on comparison to NMR data. *J. Comput. Chem.* **2019**, *34*, 2135–2145. [[CrossRef](#)]

Disclaimer/Publisher's Note: The statements, opinions and data contained in all publications are solely those of the individual author(s) and contributor(s) and not of MDPI and/or the editor(s). MDPI and/or the editor(s) disclaim responsibility for any injury to people or property resulting from any ideas, methods, instructions or products referred to in the content.